

Through-Bond Coupling | Hot Paper |

Helical Oligoenes: Conformations, Bond Alternation, and Competing Through-Bond and Through-Space Transmission

Yuta Tsuji and Roald Hoffmann*^[a]

Abstract: There is a consensus that long-range electron transfer/transport occurs by a through-bond rather than through-space mechanism. In helical all-*Z*, all-*s-cis* oligoenes, one can set up an interesting competition in the medium-separation regime between a closer (in distance) through-space path and a more distant through-bond one. Although such oligoene conformations/isomers are unstable (by around 4 kcal mol⁻¹ per double bond relative to all-*E*, all-*s-trans* isomers), recent synthetic efforts on truncated helicenes and oligothiophenes have provided related molecules. On the way to transmission calculations with electrodes attached to the termini of helical oligoenes, we uncover an interesting conformational ambiguity in all-*Z*, all-*s-cis* oli-

goenes, the existence of a broad conformational minimum for helical compression, with hints of end-to-end frontier-orbital-caused stabilization. There is relationship between helical oligoene structures and the corresponding substructure of a helicene, but there are also significant differences in the number of olefin subunits per helix turn. In Hückel transport calculations, the role of TB or TS mechanisms is obscured to an extent by variations in bond alternation and dihedral angle along the oligomer chain. However, the operation of a dominant through bond mechanism emerges clearly in local transmission plots. In moving the electrodes to carbon position related by quantum interference, it is possible to uncover a through space mechanism.

Introduction

Interactions between two localized orbitals or groups of orbitals in a molecule can be thought of as direct through-space (TS) and indirect through-bond (TB).^[1,2] The distinction may be theory-laden and is never unambiguous, yet it is useful. The most striking manifestation of the contrast (through-bond vs. through-space) is when an interesting counterintuitive orbital-level ordering ensues as a consequence of TB coupling, one in which the in-phase combination of the orbitals in question is more destabilized than the out-of-phase one. Many experiments have been conducted to assess the chemical and physical significance of these interactions.^[3] For example, measurements of the ionization potentials of non-interacting π -bonds (by photoelectron spectroscopy) can shed light on the mode of interaction between them.^[4,5]

One way to probe the TS vs. TB interaction dichotomy is to examine how interactions are affected by the distance between the two coupling moieties. Generally, the decay of the TS interaction, often gauged through an overlap integral vs. distance dependence, is much faster than that of the TB interaction.^[6] A good measure of the decay of these interactions is found in electron transfer/transport processes in donor-bridge-acceptor or electrode-molecule-electrode arrays.

The decay, whether TS or TB, has been shown experimentally and theoretically to be exponential. The distance dependence of the electron transfer rate constant k_{ET} in the superexchange mechanism is described as follows:^[7]

$$k_{\text{ET}} = k_0 \exp(-\beta_{\text{ET}}d) \quad (1)$$

where k_0 is a kinetic prefactor. Similarly, in the coherent off-resonant tunneling transport regime, the conductance g shows an exponential falloff behavior with respect to the transport distance d , as follows:^[8]

$$g = g_0 \exp(-\beta_{\text{C}}d) \quad (2)$$

where g_0 is a constant prefactor. In Equations (1) and (2), the decay process can be characterized by the exponential decay factors β_{ET} and β_{C} . The smaller the β value is, the more rapidly and efficiently electron transfer/transport can occur. The β value for TB processes can be expected to be smaller than that for TS processes.

There are various ways to characterize the space between electronic probes. Thus Beratan and co-workers proposed a tunneling path model to divide the donor-acceptor interaction in electron transfer inside proteins into covalent-bond (TB), hydrogen-bond, and TS contributions.^[9] Curtiss and co-workers suggested a superexchange pathway model and investigated the contribution of the TB and TS electronic-coupling interactions in electron transfer mediated by cyclohexane bridges.^[10] The decay factor is determined by the balance of TS and TB contributions over relatively short distances, but for

[a] Dr. Y. Tsuji, Prof. Dr. R. Hoffmann
Department of Chemistry and Chemical Biology, Cornell University
Baker Laboratory, Ithaca, NY 14853 (USA)
E-mail: rh34@cornell.edu

Supporting information for this article is available on the WWW under <http://dx.doi.org/10.1002/chem.201600042>.

long-range electron transfer processes the TB coupling emerges as the dominant mechanism.^[11,12]

Joachim and co-workers^[13] introduced the TS vs. TB dichotomy into molecular junctions, that is, electrode–molecule–electrode systems. They defined the TS and TB processes as electron tunneling from one electrode to the other without any interaction with the molecule, and electron tunneling between the two electrodes using the specific tunneling path provided by the molecule, respectively. Their tight-binding calculations showed that if the molecule is long enough, TS tunneling vanishes, as for electron transfer. They also investigated the transition of transport from a TS to a TB coupling regime, based on theoretical calculations for molecular junctions consisting of a gold atomic wire.^[14] They concluded that when the atomic wire is longer than three atoms, TS couplings become negligible.

The difference between TB and TS contributions to molecular conductance may be probed experimentally. For example, Majda and co-workers^[15] measured current through a self-assembled monolayer (SAM) of alkanethiols. In the perpendicularly oriented (relative to an underlying surface) alkanethiol monolayers, the TB pathway should be dominant. As the chains tilt, an additional pathway including a chain-to-chain coupling, which Majda and co-workers defined as a TS pathway, should play an important role. They estimated the exponential decay factors for the TB and TS pathways to be 0.91 \AA^{-1} and 1.31 \AA^{-1} , respectively.

Another insight into the competition between TB and TS mechanisms can be obtained from measurements of the force/current relationship through a singly bonded SAM using conducting-probe atomic force microscopy (CP-AFM). The stronger coupling between the molecule and the AFM tip, which is reflected as the measured force, can be expected to change the mechanism from TS to TB.^[16,17] The coupling strength between the molecule and electrode, which can modulate the balance between TS and TB contributions, can also be studied by changing anchoring units.^[18]

Recently, destructive quantum interference (QI) in molecular conductance has attracted broad interest. Here π -type TB transmission between specific pairs of atoms in π -conjugated molecules is significantly attenuated as a result of purely quantum mechanical aspects of electron transport.^[19,20] When QI occurs, the remaining transmission can be regarded as σ -type TB transmission and/or TS transmission.^[21,22]

The difference between TB and TS transport mechanisms may also be probed theoretically. For example, the peaks in transmission spectra can be informative: TB tunneling is characterized by broad peaks, but TS resonance tunneling by sharp narrow peaks.^[23] The spatial distributions of molecular orbitals (MOs) obtained from a molecular projected self-consistent Hamiltonian states (MPSH) analysis can also be informative: TS resonance tunneling is likely to occur in systems with rather localized frontier MOs.^[18] The variation between the TS and TB transport pathways can be strikingly visualized by plotting local currents.^[24]

Recently we calculated the transmission probabilities for 1–2 and 1– N electrode attachment in an [N]annulene with bond

length alternation.^[25] As a consequence of bond alternation, which is likely to affect only the TB (here the π -bonds along the polyene chain) process, the 1– N transmission is strongly attenuated, despite the fact that both connections (1–2 and 1– N) have nearly the same electrode-to-electrode distance. The local transmission plots for [14]annulene junctions support our reasoning.

Herein we undertake a study of helical all- Z , all- s - cis oligoenes to investigate whether the transmission follows a well-demarcated system of π bonds (TB mechanism), over a longer separation, or a shorter-distance path (TS mechanism).

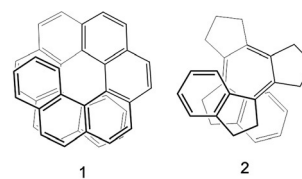
Results and Discussion

Polyacetylenes, helicenes, and all- Z all- s - cis oligoenes

Polyacetylene (PAC), or polyene, may exist in various geometrical isomeric forms, named as *trans-transoid* (all- E , all- s -*trans*), *trans-cisoid* (all- E , all- s -*cis*), *cis-transoid* (all- Z , all- s -*trans*), and *cis-cisoid* (all- Z , all- s -*cis*).^[26] The *cis-cisoid* conformation is expected to have a helical structure, but the parent system has not yet been prepared reproducibly. Kaneko and co-workers reported the synthesis of a *cis-cisoid* PAC that is stabilized by hydrogen bonds between the side groups.^[27,28] There are many theoretical studies which make a comparison between *cis* and *trans* isomers of the linear PACs,^[29–32] but there are few studies of helical ones. A density functional theory (DFT) calculation by Tasumi and co-workers^[33] showed that the potential-energy curve for *cis-cisoid* conformation has a shallow local minimum and is the most unstable of the four forms named above.

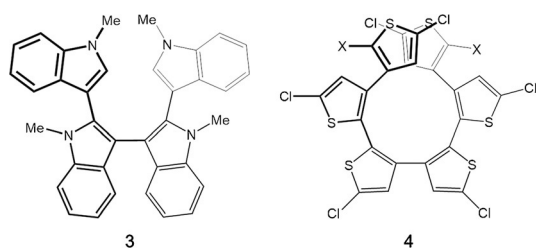
Helicenes^[34,35] are a fascinating organic architecture in which benzene rings, extended in a “phenanthrene” way, are soon forced to form a helix (exemplified here by a [9]helicene, **1**). Recently they have attracted much attention for their potential application as spring-like molecular devices whose electronic properties can be easily tuned by mechanical force. Vacek et al. theoretically demonstrated that stretching or compressing of a helicene placed between two gold electrodes significantly affects its conductance and thermopower.^[36] Guo et al. investigated the current flow through helicenes under stretching and compression, and found a U-shaped curve of the current against the pitch of a helicene.^[37]

Of tremendous variety and interest in and of themselves, helicenes also contain in their structures an all- Z , all- s - cis oligoene. Werz and co-workers^[38,39] have reported the synthesis of a novel modification of the helicene framework, in which the π -system is truncated to just the all- Z oligoene chain of interest to us (exemplified here by **2**). They call these remarkable molecules “helicenes truncated to a minimum”. Werz et al.



have successfully synthesized all-*Z* diene, triene, and tetraene encased in such systems.

Such helical structures can also be prepared by using a heterocycle as a building block. Cui and Kertesz predicted the stability of helical conformations of polythiophene, polypyrrole, and their derivatives based on semi-empirical crystal orbital calculations.^[40] Mahato and co-workers^[41] synthesized a tetramer of indole, **3**, the X-ray structure of which shows a helical conformation. Marsella and co-workers^[42–44] synthesized sexithiophene, **4** (X=H, Cl, or Br), and its X-ray structure confirmed a predicted helical conformation. This helical structure exhibits redox-induced conformational changes. Marsella and co-workers proposed that such helical molecules have the potential of acting as molecular muscles, actuators, and rheostats.^[45] The double bonds in the oligothiophenes and indoles are a part of hetero-aromatic rings, so they are severely constrained; still it is worthwhile to compare them with helical oligoenes. There are also other theoretical^[46,47] and experimental^[48–52] studies of helical molecules in the literature.



Herein we model all-*Z*, all-*s-cis* hexatriene, octatetraene, decapentaene, and dodecahexaene, and are led at one point to look at some of the truncated helicene parents as well as helical oligo-indoles and -thiophenes. We will call the simple oligoene molecules helical oligoenes HOE(*N*), where *N* is the number of double bonds, which, in turn, can be regarded as a measure of the through- π -bond distance. We study electron transmission through these helical oligoenes with the non-equilibrium Green's function (NEGF) method.^[53] The reason for examining these architectures is obvious. End-end probes in the helical geometry set up a competition between a shorter TS distance, but a longer TB path, even as the latter offers up a better, if attenuated, transmission. Which will win?

An unexpected complexity for all-*Z* all-*s-cis* oligoene conformations

On the basis of the crystallographic structures of **5** and **6** (E = CO₂Me),^[54] we optimized the simpler oligoene-skeleton model structures embedded in the known molecules, namely HOE(*N*), at the B3LYP-D3BJ/6-311 + +G(d,p) level of theory (Grimme's D3 dispersion correction with the Becke and Johnson damping function). The details of the methods used are given in the Theoretical Methods section below. In the crystal structures, both left-handed and right-handed helices are present. We adopted the left-handed one.

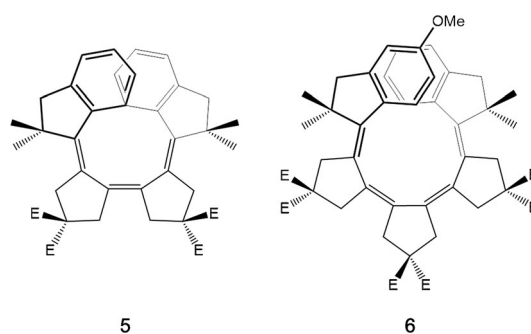


Figure 1 shows the optimized structures for HOE(3) and HOE(4) as well as the experimental crystal structures of **5** and **6**. When we compare HOE(3) with **5**, we do not find any significant difference, especially in bond length alternation, despite the excision of the bulky side groups in the oligoene model.

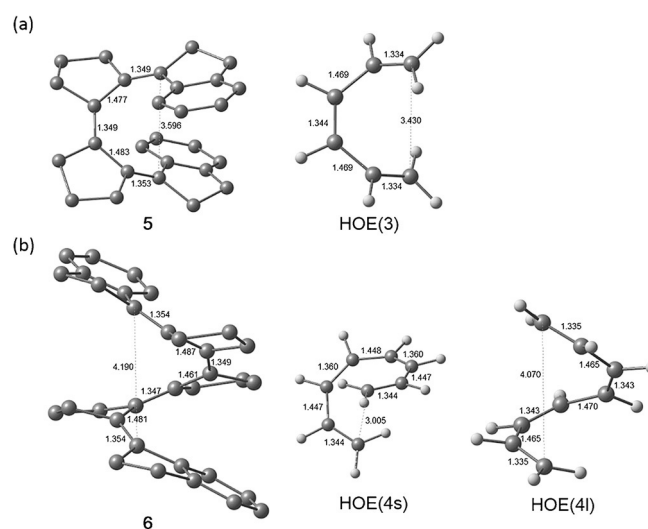


Figure 1. X-ray crystallographic structures of **5** and **6**, where hydrogen atoms and bulky side groups are omitted for simplicity (left), and B3LYP-D3BJ/6-311 + +G(d,p) optimized structures for a) HOE(3) and b) HOE(4) (right). Selected C–C distances [Å] are shown.

In the case of HOE(4), all-*Z*, all-*s-cis* octatetraene, we obtained, surprisingly, two optimized structures. We will call the structures with the shorter and longer end-to-end distances HOE(4s) and HOE(4l), respectively. HOE(4s) is more stable than HOE(4l) by 1.9 kcal mol⁻¹ (1.2 kcal mol⁻¹ if the dispersion correction is not included in the computation). But the observed crystal structure is closer to the HOE(4l) model. The degree of bond alternation in the crystal structure is also closer to HOE(4l), as will be discussed later. The large differential between the geometries of HOE(4s) and HOE(4l) is in the dihedral angles along the chain, which are shown in the Supporting Information.

For comparison, Figure 2 shows the crystal structure of **3** and **4** (X=H). They can be viewed as tetraenes. The distance between terminal carbon atoms in the helical skeleton in **3** is close to that of HOE(4l). That in **4** depends on X, and is in the

structures with two functionals considered to be better, M06-2X and ω B97X-D. The optimum geometries of both HOE(4s) and HOE(4l) calculated with these methods were close to what was given by the B3LYP-D3BJ functional. And now the energies of the minima were within 0.2 kcal mol⁻¹ of each other (details in the Supporting Information).

We then carried out CCSD(T) single point calculations for the minimum energy geometries with both functionals. Now the HOE(4s) structure emerged 1.1 to 1.2 kcal mol⁻¹ less stable than the long C–C conformer.

We think a trustworthy conclusion is that in these molecules there is a broad region of the potential energy surface for helical compression that is of very similar energy. Whether a given molecule settles in one or another geometry may be a consequence of crystal packing.

3. Why a broad minimum should exist

A glance at the geometry of HOE(4s) shows that it is abnormal, not the long isomer. For the end carbons are only 3.0 Å apart, to be compared with the graphite van der Waals minimum interlayer spacing of 3.4 Å. There is some attractive interaction at work here.

Figure 6 shows the highest occupied molecular orbital (HOMO) of HOE(4s). We can expect a substantial p_σ–p_σ bonding interaction. It will be counteracted by a corresponding antibonding interaction in the HOMO–1, but that is expected to be smaller, as the orbital lies 0.9 eV lower. In fact the helical geometry is close to the optimum geometry for an electrocyclic closure, to a cyclooctatriene. And that reaction has a computed activation energy that is very small (around 2.5 kcal mol⁻¹^[55]). On the other hand, in HOE(4l), the long minimum, the distance between the C1 and C7 atoms is 3.5 Å. At this separation, the p_σ–p_σ bonding interaction should be weaker than HOE(4s), but, as Figure 6 shows, the p_σ–p_σ bonding interaction exists not only between the C1 and C7 atoms but also between the C2 and C8 atoms. Perhaps this can explain why HOE(4l) has a shallow minimum.

In the case of oligothiophene **4**, the π orbitals of the terminal thiophenes are not included in the helix but can interact

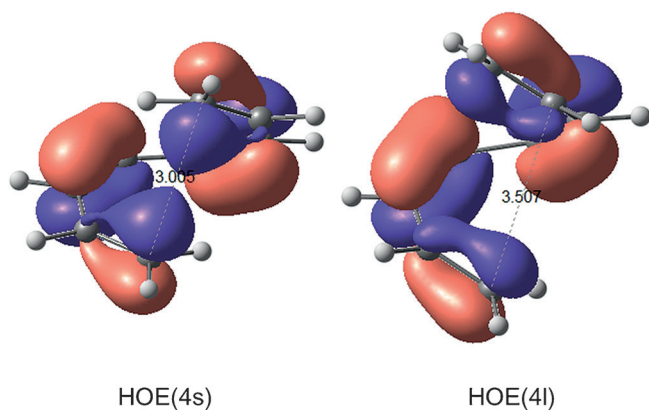


Figure 6. HOMO of HOE(4s) and HOE(4l) calculated with B3LYP-D3BJ/6-311++G(d,p).

with the π-orbitals of the helical skeleton, leading to a p_σ–p_σ antibonding interaction in the HOMO (see the Supporting Information). This is why the oligothiophene helices have longer C1–C8 distances. In the oligothiophene helices an electrocyclic closure cannot be expected.

Having outlined the reasoning that leads us to accept the presence of a broad energy minimum with respect to helical compression for the all-Z, all-s-cis oligoenes we return to more realistic models, the truncated helicenes synthesized.

For molecule **6**, with its full complement of substituents, no replacement of any atoms by Hs, at the B3LYP-D3BJ/6-31G(d) level of theory, one gets the potential energy curve shown in Figure 7. Interestingly, there are still two minima. The dispersion correction makes quite a difference here, as curves in the Supporting Information shows.

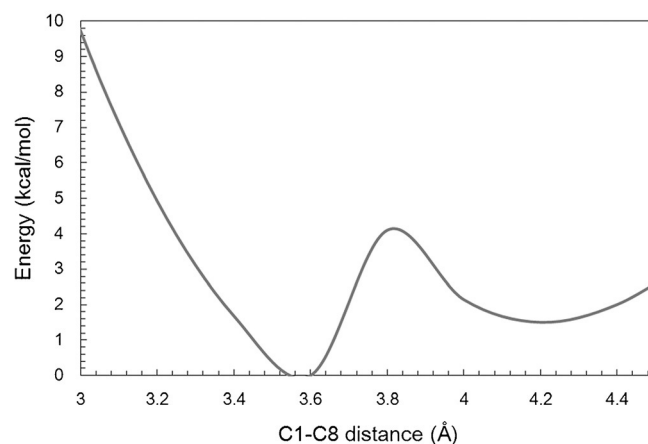


Figure 7. Calculated potential energy curve as a function of the distance between the C1 and C8 atoms for **6** at the B3LYP-D3BJ/6-31G(d) level of theory.

For the full structure, the long end-to-end distance minimum (at 4.2 Å) is not as shallow as it was for HOE(4). Clearly, the truncated helicene side groups sculpt the surface in distinct ways. The greatest influence is exerted by the methyl groups attached to the five membered ring of the terminal indane groups (see the Supporting Information). The reported crystal structure (Figure 1b) has a C1–C8 distance of 4.19 Å, close to the long minimum. Interestingly, there is in the observed crystal structure a second molecule in the asymmetric unit, with C1–C8 4.46 Å, also long.

On the other hand, in the cases of **3** and **4** (X=H) the similarly calculated potential energy curves have only one broad minimum, as shown in the Supporting Information. The potential energy curves of helicenes also have a single minimum, which can be nicely approximated by a parabola.^[56,57] A helicene under stretching or compression by two gold-electrode surfaces also has a potential energy curve with only one broad minimum.^[36] However, the potential energy curve of helical polyisocyanides calculated as a function of helical angle by the extended Hückel method has two minima.^[58]

Should we take the (deeper) short C1–C8 minimum for truncated helicene **6** seriously? We do not have the computational

resources for a CCSD(T) calculation on **6**. Given what we found for HOE(4), we would like to withhold judgement on the above question. But there may be a polymorph of **6** waiting to be made.

The relationship between HOEs and helicenes

We know that there is a helical oligoene hiding in a helicene. And we also know that in a helicene, the π -bonding in the HOE part of the helicene is aromatic, delocalized, and in that way different from the bonding in an HOE. Are there structural consequences of this difference?

It is natural to focus a comparison on the pitch of the helix. Mathematically, the pitch is defined as the width of one complete helical turn measured parallel to the axis of the helix.^[59] Unlike the mathematical model, helical molecules are built up from atoms, with definite positions. One may define the pitch of helical molecules as the distance from one atom to another atom positioned directly above the first one, in the next turn of the helix. However, the problem is that sometimes no atoms can be found directly above. Therefore, we need some approximate measure of the pitch in helical molecules.^[47] One such way is to use the shortest through-space C–C distance across one turn.

In the case of helicenes, we can use for the pitch the distance from one atom to another atom positioned directly above the first one in the next turn, because there is a good overlap of atoms between the one turn and the next turn, as seen in an isometric projection of a [16]helicene structure^[35] in Figure 8a; we can see a hexagon-shaped overlap of atoms. The number of benzene rings per helix turn is approximately rational, equal to 6. The C_{n+6} atoms are located just above the C_n atoms. The pitch can be defined as the distance between these atoms. In Figure 8b some such distances for the outer helix of helicene are shown. They are in the range from 3.5 to 4.2 Å. On the other hand, in the case of the inner helix, which is the structural segment of the helicene analogous to

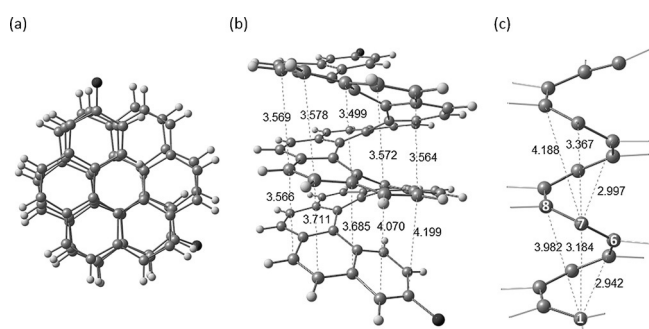


Figure 8. a) Top view (isometry) of the X-ray crystal structure of [16]helicene.^[35] The black spheres indicate the terminal group (–OSiCH(CH₃)₂). b) Side view of the [16]helicene. The distances in Å from one atom to another atom in the next turn positioned almost directly above the first one in the outer helix are shown. c) Side view of the inner helix of the helicene. Selected C–C distances between C_n and C_{n+5} , C_{n+6} , and C_{n+7} are shown in Å.

the model helical oligoenes, the pitches are little bit shorter than those in the outer helix, as shown in Figure 8c.

Now let us look for the pitch of optimized helical oligoenes. Since even HOE(6) includes only one and half turns in the helix, we optimized the structure of HOE(12), so that we can see a few turns. B3LYP does not give any local minimum for HOE(12I), while M06-2X gives both HOE(12s) and HOE(12I) minima, as shown in Figure 9. HOE(12I) is more stable than HOE(12s) by 2.2 kcal mol^{−1} at the M06-2X/6-31G(d) level of theory, but we are hesitant to accept this value, since B3LYP does not agree with M06-2X results in this case. And we do not have the computational resources to study the potential energy surface between the long and short isomers.

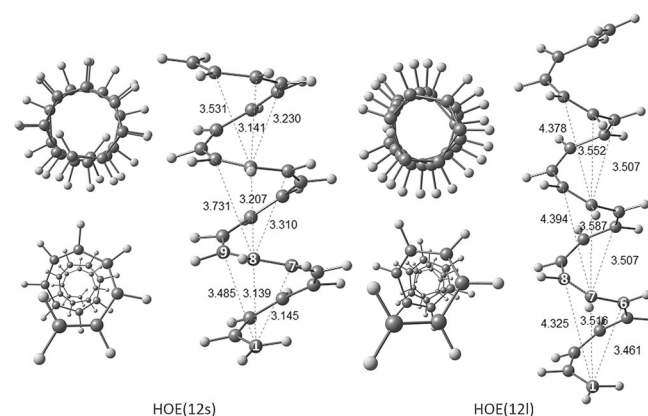


Figure 9. Isometric top view, perspective top view, and side view of HOE(12s) (left) and HOE(12I) (right) optimized at the M06-2X/6-31G(d) level of theory. Selected CC distances between C_n and C_{n+5} , C_{n+6} , C_{n+7} , and C_{n+8} are shown in Å.

As the isometric projection along the helix axis shows at a glance, the HOEs are different from the helicenes; the number of double bonds per helix turn is not rational. Still one can estimate a pitch by the shortest through-space C...C distance across approximately one turn. We use the distance between C_n and C_{n+7} for the pitch. The pitch for HOE(12s) is then around 3.1–3.2 Å.

Let us try another, more mathematical way to describe the pitch of the HOEs. First of all, we need a definition of the helical axis for helical molecules, the component atoms of which are specified by Cartesian coordinates. One reasonable definition may be the line for which the root mean square distances from the line to the component atoms of the helix are minimized. We obtained such a line by using the best-fit line option implemented in Materials Studio.^[60] We use \mathbf{u} for the unit vector of the helical axis and \mathbf{v}_x for the vector from C_n to C_{n+x} . Then the pitch p can be approximated by the scalar projection of \mathbf{v}_x in the direction of the helical axis \mathbf{u} as follows:

$$p = \mathbf{v}_x \cdot \mathbf{u} = \|\mathbf{v}_x\| \cos \theta \quad (3)$$

where $\|\mathbf{v}_x\|$ is the magnitude of the vector \mathbf{v}_x , that is, the distance between C_n and C_{n+x} , and θ is the angle between \mathbf{v}_x and \mathbf{u} . C_{n+x} should be chosen so that θ is minimized. In the

case of HOE(12s), x should be 7 because the angle between \mathbf{v}_7 (the vector from C1 to C8) and \mathbf{u} is 9.0° , but those between, for instance, \mathbf{v}_6 and \mathbf{u} and between \mathbf{v}_8 and \mathbf{u} are 32.3° and 15.5° , respectively. Since $\cos 9.0^\circ = 0.99$, $p \approx ||\mathbf{v}_x||$, which means the “atomistic” definition of the pitch is consistent with the more sophisticated vector-based definition.

The shortest through-space C...C distance across one turn in HOE(12l), the stretched conformer, is the distance between C_n and C_{n+5} , but the line between these atoms is clearly slanted with respect to the helical axis ($\theta = 24.9^\circ$). Since the line between C_n and C_{n+6} is almost parallel to the helical axis ($\theta = 2.0^\circ$), and these atoms appear almost overlapped in the top view, it would be better to define their separation as the pitch. The pitch is then around 3.5–3.6 Å. Therefore, the helical structure of the inner helix of helicene is more similar to HOE(Nl) than HOE(Ns).

The Supporting Information, Section S7, contains another approach to the problem of multiple conformational minima. There we construct two ideal helices, with a rational number of repeat units per turn, six or eight (so that their projections down the helix axis show hexagons or octagons). Their potential energy curves resemble the short and long minima we find for real helical oligoenes.

To summarize: helical oligoenes, whether in a long or a short conformer, are quite different from helicenes in two ways: 1) The helix in the HOEs, whether l or s, has an irrational number of repeat units (ethylenes) per turn; that number is between 3 and 4. The l conformer is closer to the helicene; and 2) the HOE helix shows signs of ethylene-ethylene attraction in the short conformer, with a smaller pitch, as approximately as that pitch is defined. And, naturally, there is no bond alternation along the inner HOE part of the helicene.

The energetics of oligoenes

At this point it is useful to put the model HOE(N) structures in context by looking at alternative oligoene structures. There are many local minima on the $C_N H_{N+2}$ surface. If we use the standard notation of *E* and *Z* for isomerism with respect to localized (we will see how localized below) double bonds, and *s-cis* and *s-trans* for conformations around single bonds, one can have the extreme isomers/conformations shown in Figure 10.

Despite the steric repulsion between two Hs on C1 and C4 atoms, all-*Z*, all-*s-trans* isomers keep the planar geometry. On the other hand, in the case of all-*E*, all-*s-cis* isomers, such steric repulsion between the H atoms can be reduced by a moving out of planarity. This happens in the archetype, butadiene. Figure 11 shows the energetics of these 4 isomers/conformations as a function of N . The reference line is the global minimum, the all-*E*, all-*s-trans* oligoene. The Supporting Information also shows the computed HOMO–LUMO gaps for all isomers.

Not unexpectedly, the order of stability is all-*E*, all-*s-trans* > all-*Z*, all-*s-trans* > all-*E*, all-*s-cis* > all-*Z*, all-*s-cis* (short) > all-*Z*, all-*s-cis* (long). Note how the various stability lines extrapolate nicely to butadiene; the destabilization of *s-cis* conformations clearly cumulates. The destabilization of the HOE(N) isomers is

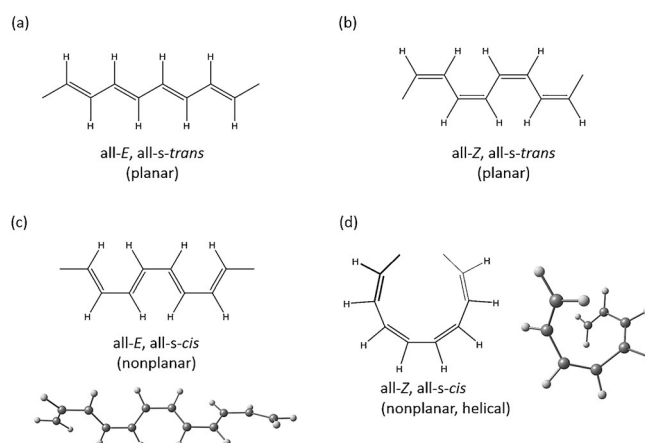


Figure 10. Four isomers/conformations of oligoenes (polyenes). (a) all-*E*, all-*s-trans*, (b) all-*Z*, all-*s-trans*, (c) all-*E*, all-*s-cis*, and (d) all-*Z*, all-*s-cis* isomers.

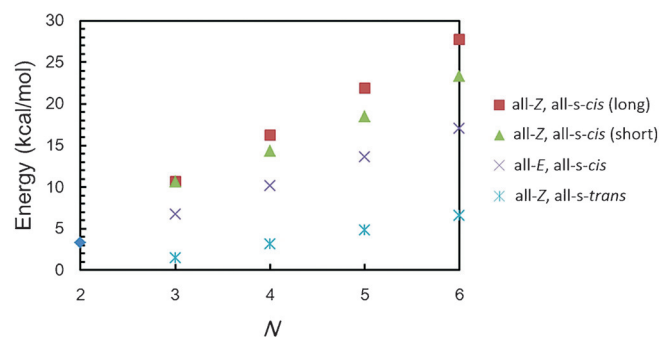


Figure 11. Relative energies of the oligoene isomers/conformations to the global minimum, the all-*E*, all-*s-trans* oligoene as a function of N . The blue diamond on the y axis indicates the relative energy of *s-cis* butadiene (nonplanar) to *s-trans* butadiene. These energies were calculated at the B3LYP-D3BJ/6-311++G(d,p) level of theory.

substantial, 4–6 kcal mol⁻¹ per double bond, and rising with N . One is tempted to attribute this destabilization to the strain of the enforced helical geometry. But at the same time we saw a stabilizing factor in the shortened (relative to a graphite separation) 1,2*N*-distance in the short end-to-end length isomer of these molecules. This attraction is insufficient to overcome overall strain of a helical geometry. It is apparent (as it was without any calculations) why the double bonds in the HOEs had to be incorporated into rings to be experimentally realized.

Bond alternation

A difference between single and double bond lengths is expected for all oligoenes, and, going back to seminal work by Salem and Longuet-Higgins,^[61] should persist in the infinite N limit, the so-called polyacetylene. As we will see, bond alternation affects strongly the measure of coupling between the ends of the oligoene that we choose to consider, electron transmission through molecules. So it is important to look at this bond alternation in oligoenes.

Bond alternation can be gauged in a number of ways. One measure could be the difference between the average long and short carbon–carbon bonds in a conjugated molecule:^[62]

$$\delta = \bar{R}_{\text{long}} - \bar{R}_{\text{short}} \quad (4)$$

There are other measures that have been reported.^[63,64]

Figure 12 shows the bond alternation measure δ for the computed oligoene isomers/conformations. Generally the degree of bond alternation decreases with an increase in the number of double bonds, and seems to be headed for an asymptotic limit, as expected. The degree of bond alternation calculated from the experimental structures of all-*trans* polyacetylene is in the range between 0.07 and 0.09.^[62] The calculated degree of bond alternation for HOE(N) is larger than that in HOE(Ns), and is consistent with the alternation observed in the X-ray crystal structures of **5** ($\delta=0.130$) and **6** ($\delta=0.125$, 0.135). The degree of bond alternation in all-*trans* oligoenes takes an intermediate value between HOE(Ns) and HOE(NI). We are not sure what to make of the difference in bond alternation between the oligoene Ns and NI structures.

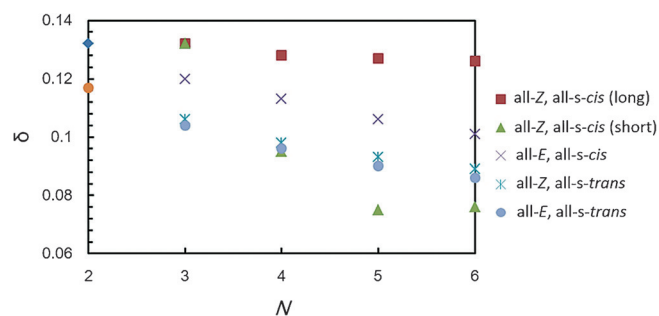


Figure 12. Bond alternation measure δ for the computed oligoene isomers/conformations at the B3LYP-D3BJ/6-311 + + G(d,p) level of theory as a function of N . The blue diamond and orange circle on the y axis indicate the values of δ for *s-cis* butadiene and *s-trans* butadiene, respectively.

Electron transport through all-Z oligoenes

Our first attempt to establish the TB or TS nature of end-to-end transmission in HOEs was with the Hückel model used previously.^[25,65,66] The bond alternation in an oligoene (and we observed that bond alternation above) causes an exponential falloff of the conductance in a system of N double bonds, according to Equation (5):

$$g = g_0 \exp[-\{2 \ln(\beta_D/\beta_S)\}N] \quad (5)$$

where β_D and β_S are the Hückel resonance integrals in a double and single bond. The ratio can be estimated from a Mulliken relationship of β to the overlap integral S .

The transmission is further affected by the dihedral angles around the single bonds; these range from 6 to 55° in the HOEs. The net effect of bond alternation and dihedral angles in a Hückel model is inconclusive; there is no obvious correla-

tion of end-to-end conductance with either TS or TB distance. The details are provided in the Supporting Information.

A clearer picture through local transmission plots

For another perspective on the TB vs. TS dichotomy, we use a local transmission analysis,^[67] based on wave functions computed at the DFT level. In contrast to the Hückel calculation, the DFT Hamiltonian, or Fock matrix, and the overlap matrix include almost all the electronic and geometric information, such as bond alternation, dihedral angles, non-nearest-neighbor interactions, and σ electrons.

DFT calculations for realistic molecular junctions require anchoring groups that can connect the molecule with the electrodes. In our calculations HOE(N) molecules are linked to gold clusters using ethynylthiol groups ($-\text{C}\equiv\text{C}-\text{SH}$). The terminal carbon atom in HOE(N) has two hydrogen atoms, which can be replaced with the linker. Assuming C_2 symmetry, there are, in principle, three configurations for linker replacement, namely (*E,E*), (*E,Z*), and (*Z,Z*). After adding the linker groups we reoptimized the geometry. For $N \geq 4$ the geometry optimizations of HOE(Ns) and HOE(NI) with the linker groups result in the same geometry, whose helical π -conjugated skeleton is closer to that of the original HOE(Ns) structure. We will call these reoptimized structures with the linker groups (*E,E*)-HOE(N), (*E,Z*)-HOE(N), and (*Z,Z*)-HOE(N). Given the size of the linker and electrode model, some geometries are sterically impossible: for (*E,Z*)-HOE(3), (*E,E*)-HOE(4), and (*Z,Z*)-HOE(5), carbon atoms bump into the electrodes.

Figure 13 shows the local transmission plots for the 1–2*N* connections of HOE(N). The diameter of the arrows in Figure 13 represents the value of the local transmission for a pair of atoms. Here we chose one linkage isomer for each oligoene, (*Z,Z*), except for HOE(5), where the (*Z,Z*) structure is impossible, and where we substitute (*E,E*). All isomers are shown in the Supporting Information. Although we can see very small TS contributions, which are indicated by arrows connecting atoms between which no bond is formed, the dominant mechanism is very clearly TB (see the difference in thickness of the arrows between TB and TS transmissions).

Since we can see a loop current in most of the structures, which might produce a magnetic moment, might such molecules be candidates for a molecular solenoid?^[68]

It is possible to switch the dominant transport mechanism from TB to TS. Given the general dominance of the TB mechanism, the electrode placement that might give a TS mechanism a chance is where quantum interference annihilates the through- π -bond transmission. In an oligoene, one place where this occurs is when the first and $2N-1$ th atoms are connected to the electrodes.^[66] The residual transmission that one is likely to observe can come from through- σ -bond and TS mechanisms. The contributions of σ -transmission are likely to become smaller as the molecule gets larger.^[21,69]

A reviewer has suggested that there is another way to switch from TB to TS dominance, and this is by increasing the degree of bond alternation, thus having the TB transmission

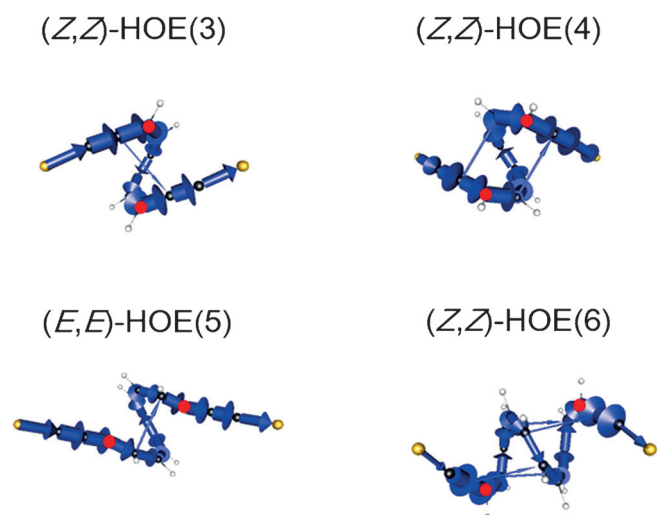


Figure 13. Local transmission plots for the 1–2*N* connections of HOE(*N*). The first and 2*N*th carbon atoms are indicated by red dots. Total transmission at the Fermi level is decomposed. The local transmission contributions are depicted only if above a threshold value of 0.05. The diameter of the arrows is proportional to the value of the local transmission for a pair of atoms. Sulfur atoms bonded to Au electrodes (not shown) are shown in yellow.

fall off faster. This suggestion makes sense; we explore it in the Supporting Information, Section S11.

Since the first carbon atom has two hydrogen atoms but the 2*N*–1th carbon atom has only one hydrogen atom, there are, in principle, two configurations for placement of the linker to the electrodes, namely *E* and *Z*. We will call the resulting two isomers (*E*)-HOE(*N*) and (*Z*)-HOE(*N*), respectively. Again, the re-optimized structure of HOE(*N*s) and HOE(*M*) with the linker groups converged to the same structure, which is closer to that of HOE(*N*s). Also again, some are sterically impossible: (*Z*)-HOE(3), (*Z*)-HOE(4), and (*E*)-HOE(5). Figure 14 focuses on two typical oligoenes: (*Z*)-HOE(5) and (*E*)-HOE(6); the full set of isomers is shown in the Supporting Information.

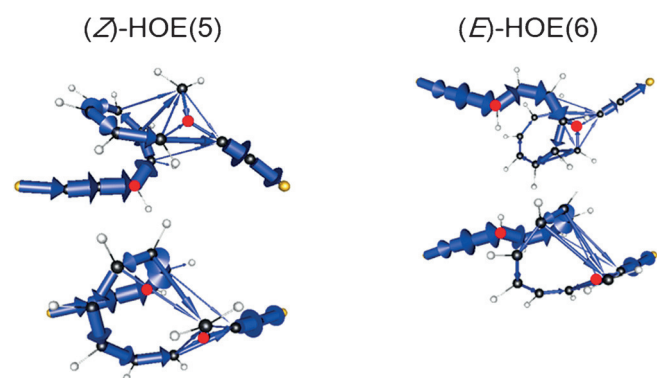


Figure 14. Local transmission plots for the 1 to 2*N*–1 connections of (*Z*)-HOE(5) and (*E*)-HOE(6). The first and 2*N*–1th carbon atoms are indicated by red dots. For each structure two views taken from different angles are shown. Total transmission at the Fermi level is decomposed. The local transmission contributions are depicted only if above a threshold value of 0.05. The diameter of the arrows is proportional to the value of the local transmission for a pair of atoms. Sulfur atoms bonded to Au electrodes (not shown) are shown in yellow.

The transmission plots are complicated; one can see a TB transmission sequence from carbon 1 to carbon 2*N*–2. Then the final step from C2*N*–2 to C2*N*–1 is much attenuated. Instead there are a number of TS transmission paths, stronger than any shown in Figure 13 to C2*N*–1 and C2*N*.

We also carried out detailed DFT calculations of the transmission for 1,2*N* and 1,2*N*–1 electrode attachment. Consistently, the 1,2*N* transmission was at least an order of magnitude higher than the 1,2*N*–1 one. Typical values are $1.6\text{--}1.7 \times 10^{-2}$ for HOE(6) 1–2*N* (the range is for different stereochemistry of attachment) vs. $7.0\text{--}7.2 \times 10^{-4}$ for the same oligoene, electrodes 1,2*N*–1. The 1,2*N*–1 transmissions correlate with the TS distance between electrodes; no such correlation is calculated for 1,2*N* transmission.

Summary and Conclusion

Helical oligoenes offer an opportunity, in principle, to set against each other through-space and through-bond mechanisms for electron transport. And recently synthesized molecules give us a realization of these structures. We investigated the structures of all-*Z*, all-*s-cis* helical conformations of oligoenes and found, unexpectedly, a range of pretty much equal energy structures for tetraene, pentaene, and hexaene varying in helix pitch. An intramolecular orbital interaction stabilizes a more compact conformation in the higher helical oligoenes.

We even investigated a 12-ethylene helix, so as to make a correlation (there in part, yet with significant differences) with the oligoene substructure of a helicene.

Detailed calculations on alternative all-*Z* and all-*E* oligoene conformers/isomers show the energetic destabilization, about 4–6 kcal mol^{–1}/ethylene of the all-*Z* all-*s-cis* molecules, and the degree of bond alternation in these as they converge on polyene (polyacetylene).

We carried out Hückel and DFT electron-transport calculations for a simplified model of helical oligoenes to determine whether the dominant transport mechanism is through-space or through-bond. The Hückel calculation is indecisive, but local transmission analysis in DFT calculations show clearly that the dominant mechanism is through-bond, even if the through-space path is much shorter than the through-bond one. When the electrodes are attached to the first and 2*N*–1th carbon atoms π -type through-bond electron transmission can be completely annihilated due to a quantum effect peculiar to nano-scale electron transport, which is what is called quantum interference. Then the contribution from the through-space transmission greatly increases.

Theoretical Methods

Geometry optimizations were performed with the Gaussian 09 program^[70] at the B3LYP^[71] level of theory. The 6-311++G(d,p) and 6-31G(d) basis sets implemented in the program were used for HOE(*N*) and experimental structures, **3**, **4**, and **6**, respectively. To properly account for dispersion interactions, Grimme's D3 dispersion correction with the Becke and Johnson damping function has been added.^[72] To check the reliability of the B3LYP calculations we

used M06-2X^[73] and ω B97X-D^[74] functionals. CCSD(T)^[75] single-point energy calculations were also performed for each optimized structure.

Prior to the electron transport calculations, geometry optimizations at the B3LYP-D3BJ/6-311++G(d,p) level of theory were performed for HOE(N) with ethynylthiol linkers. After the optimization, the thiol hydrogen atoms were removed and the Au₉ clusters that approximate the electrode surface were attached in accordance with the methodology shown in a recent study.^[76] The adsorption site is the fcc-hollow site. Single-point DFT calculations were carried out for the electrode-molecule-electrode junctions at the B3LYP/LanL2MB level of theory to generate the Fock and overlap matrices for electron transport calculations. We adopted a relatively smaller basis set to avoid the problem of ghost transmission^[77] and to get a clear picture of local transmission.

Electron transmission calculations and local transmission calculations were performed by using the post-processing tool Artaios^[77,78] in the framework of the wide-band limit (WBL) approximation of the NEGF method. The location of the Fermi energy is defined as the middle energy point between the HOMO and LUMO of the entire electrode-molecule-electrode system.

The non-equilibrium Green's function matrix for an electrode-molecule-electrode system can be written as follows:^[53]

$$\mathbf{G}(E) = [\mathbf{E}\mathbf{S} - \mathbf{H} - \Sigma_L - \Sigma_R]^{-1} \quad (6)$$

where \mathbf{S} is the overlap matrix, \mathbf{H} is the Hamiltonian (Fock) matrix, and Σ is the self-energy matrix. The electron transmission probability can be calculated from the following equation.^[53]

$$T(E) = \text{Trace}[\Gamma_L \mathbf{G} \Gamma_R \mathbf{G}^\dagger] \quad (7)$$

where Γ is the broadening function matrix. Both Σ and Γ , which describe the effect of electrodes, are calculated in the framework of the WBL approximation.^[77]

Acknowledgements

Y.T. thanks the Japan Society for the Promotion of Science for a JSPS Postdoctoral Fellowship for Research Abroad. Our work at Cornell was supported by the National Science Foundation through Grant CHE-1305872.

Keywords: electron transmission • helical polymers • oligoenes • through-bond coupling

- [1] R. Hoffmann, A. Imamura, W. J. Hehre, *J. Am. Chem. Soc.* **1968**, *90*, 1499–1509.
- [2] R. Hoffmann, *Acc. Chem. Res.* **1971**, *4*, 1–9.
- [3] M. Paddon-Row, *Acc. Chem. Res.* **1982**, *15*, 245–251.
- [4] R. Hoffmann, E. Heilbronner, R. Gleiter, *J. Am. Chem. Soc.* **1970**, *92*, 706–707.
- [5] E. Heilbronner, *Isr. J. Chem.* **1972**, *10*, 143–156.
- [6] T. A. Albright, J. K. Burdett, M. H. Whangbo, *Orbital Interactions in Chemistry*, Wiley, New York, **1985**.
- [7] C. Schubert, J. T. Margraf, T. Clark, D. M. Guldi, *Chem. Soc. Rev.* **2015**, *44*, 988–998.
- [8] K. H. Khoo, Y. Chen, S. Li, S. Y. Quek, *Phys. Chem. Chem. Phys.* **2015**, *17*, 77–96.
- [9] D. N. Beratan, J. N. Betts, J. N. Onuchic, *Science* **1991**, *252*, 1285–1288.

- [10] L. A. Curtiss, C. A. Naleway, J. R. Miller, *J. Phys. Chem.* **1995**, *99*, 1182–1193.
- [11] P. S. Mariano, *Advances in Electron Transfer Chemistry*, Jai Press, Greenwich, **1994**.
- [12] J. Jortner, M. Bixon, *Advances in Chemical Physics, Electron Transfer - From Isolated Molecules to Biomolecules*, Wiley-Interscience, New York, **2009**.
- [13] C. Joachim, P. Sautet, in *Scanning Tunneling Microscopy and Related Methods* (Ed.: R. J. Behm), Kluwer, Dordrecht, **1990**, pp. 377–389.
- [14] C. Joachim, X. Bouju, C. Girard, in *Atomic and Nanometer-Scale Modification of Materials: Fundamentals and Applications* (Ed.: Avouris, P.), Kluwer, Dordrecht, **1993**, pp. 247–261.
- [15] K. Slowinski, R. V. Chamberlain, C. J. Miller, M. Majda, *J. Am. Chem. Soc.* **1997**, *119*, 11910–11919.
- [16] X. D. Cui, X. Zarate, J. Tomfohr, O. F. Sankey, A. Primak, A. L. Moore, T. A. Moore, D. Gust, G. Harris, S. M. Lindsay, *Nanotechnology* **2002**, *13*, 5–14.
- [17] A. Salomon, D. Cahen, S. Lindsay, J. Tomfohr, V. B. Engelkes, C. D. Frisbie, *Adv. Mater.* **2003**, *15*, 1881–1890.
- [18] A. Fukazawa, M. Kiguchi, S. Tange, Y. Ichihashi, Q. Zhao, T. Takahashi, T. Konishi, K. Murakoshi, Y. Tsuji, A. Staykov, K. Yoshizawa, S. Yamaguchi, *Chem. Lett.* **2011**, *40*, 174–176.
- [19] C. M. Guédon, H. Valkenier, T. Markussen, K. S. Thygesen, J. C. Hummelin, S. J. van der Molen, *Nat. Nanotechnol.* **2012**, *7*, 305–309.
- [20] G. C. Solomon, D. Q. Andrews, T. Hansen, R. H. Goldsmith, M. R. Wasielewski, R. P. Van Duyne, M. A. Ratner, *J. Chem. Phys.* **2008**, *129*, 054701.
- [21] G. C. Solomon, D. Q. Andrews, R. H. Goldsmith, T. Hansen, M. R. Wasielewski, R. P. Van Duyne, M. A. Ratner, *J. Am. Chem. Soc.* **2008**, *130*, 17301–17308.
- [22] A. Batra, J. S. Meisner, P. Darancet, Q. Chen, M. L. Steigerwald, C. Nuckolls, L. Venkataraman, *Faraday Discuss.* **2014**, *174*, 79–89.
- [23] A. Staykov, Y. Tsuji, K. Yoshizawa, *J. Phys. Chem. C* **2011**, *115*, 3481–3490.
- [24] H. Löfås, R. Emanuelsson, R. Ahuja, A. Grigoriev, H. Ottosson, *J. Phys. Chem. C* **2013**, *117*, 21692–21699.
- [25] Y. Tsuji, R. Movassagh, S. Datta, R. Hoffmann, *ACS Nano* **2015**, *9*, 11109–11120.
- [26] H. Naarmann, in *Conjugated Polymeric Materials: Opportunities in Electronics, Optoelectronics, and Molecular Electronics* (Eds.: J. L. Brédas, R. R. Chance), Springer, Berlin, **1990**, pp. 11–51.
- [27] L. Liu, T. Namikoshi, Y. Zang, T. Aoki, S. Hadano, Y. Abe, I. Wasuzu, T. Tsutsuda, M. Teraguchi, T. Kaneko, *J. Am. Chem. Soc.* **2013**, *135*, 602–605.
- [28] Z. Shi, M. Teraguchi, T. Aoki, T. Kaneko, *Chem. Lett.* **2015**, *44*, 1413–1415.
- [29] T. Yamabe, K. Tanaka, H. Teramae, K. Fukui, A. Imamura, H. Shirakawa, S. Ikeda, *Solid State Commun.* **1979**, *29*, 329–333.
- [30] S. Suhai, *J. Chem. Phys.* **1980**, *73*, 3843–3853.
- [31] A. Karpfen, R. Höller, *Solid State Commun.* **1981**, *37*, 179–182.
- [32] H. Teramae, *J. Chem. Phys.* **1986**, *85*, 990–996.
- [33] S. Hirata, H. Torii, M. Tasumi, *Phys. Rev. B* **1998**, *57*, 11994–12001.
- [34] Y. Shen, C.-F. Chen, *Chem. Rev.* **2012**, *112*, 1463–1535.
- [35] K. Mori, T. Murase, M. Fujita, *Angew. Chem. Int. Ed.* **2015**, *54*, 6847–6851; *Angew. Chem.* **2015**, *127*, 6951–6955.
- [36] J. Vacek, J. V. Chocholoušová, I. G. Stará, I. Starý, Y. Dubi, *Nanoscale* **2015**, *7*, 8793–8802.
- [37] Y.-D. Guo, X.-H. Yan, Y. Xiao, C.-S. Liu, *Sci. Rep.* **2015**, *5*, 16731.
- [38] B. Milde, M. Leibelng, M. Pawliczek, J. Grunenberg, P. G. Jones, D. B. Werz, *Angew. Chem. Int. Ed.* **2015**, *54*, 1331–1335; *Angew. Chem.* **2015**, *127*, 1347–1351.
- [39] B. Milde, M. Leibelng, A. Hecht, P. G. Jones, A. Visscher, D. Stalke, J. Grunenberg, D. B. Werz, *Chem. Eur. J.* **2015**, *21*, 16136–16146.
- [40] C. X. Cui, M. Kertesz, *Phys. Rev. B* **1989**, *40*, 9661–9669.
- [41] S. B. Mahato, S. Garai, M. Weber, P. Luger, *J. Chem. Soc. Perkin Trans. 1* **2000**, 2767–2769.
- [42] M. J. Marsella, K. Yoon, A. Almutairi, S. K. Butt, F. S. Tham, *J. Am. Chem. Soc.* **2003**, *125*, 13928–13929.
- [43] A. Almutairi, F. S. Tham, M. J. Marsella, *Tetrahedron* **2004**, *60*, 7187–7190.
- [44] A. Almutairi, K. Yoon, F. Tham, M. J. Marsella, *Pure Appl. Chem.* **2006**, *78*, 777–781.
- [45] M. J. Marsella, S. Rahbarnia, N. Wilmot, *Org. Biomol. Chem.* **2007**, *5*, 391–400.
- [46] Y.-H. Tian, G. Park, M. Kertesz, *Chem. Mater.* **2008**, *20*, 3266–3277.

- [47] P. Beaujean, M. Kertesz, *Theor. Chem. Acc.* **2015**, *134*, 147.
- [48] K. Tanaka, Y. Kitahara, *Chem. Commun.* **1998**, 1141–1142.
- [49] K. Tanaka, H. Osuga, Y. Kitahara, *J. Chem. Soc. Perkin Trans. 1* **2000**, 2492–2497.
- [50] K. Tanaka, H. Osuga, Y. Kitahara, *J. Org. Chem.* **2002**, *67*, 1795–1801.
- [51] M. Miyasaka, M. Pink, A. Olankitwanit, S. Rajca, A. Rajca, *Org. Lett.* **2012**, *14*, 3076–3079.
- [52] D. Waghay, A. Cloet, K. Van Hecke, S. F. Mertens, S. De Feyter, L. Van Meervelt, M. Van der Auweraer, W. Dehaen, *Chem. Eur. J.* **2013**, *19*, 12077–12085.
- [53] S. Datta, *Electronic Transport in Mesoscopic Systems*, Cambridge University Press, Cambridge, **1995**.
- [54] CCDC 1020999 (5) and 1021001 (6) contain the supplementary crystallographic data for this paper. These data are provided free of charge by The Cambridge Crystallographic Data Centre.
- [55] R. Hoffmann, D. J. Tantillo, *Angew. Chem. Int. Ed.* **2003**, *42*, 5877–5882; *Angew. Chem.* **2003**, *115*, 6057–6062.
- [56] M. Jalaie, S. Weatherhead, K. B. Lipkowitz, D. Robertson, *Electron. J. Theor. Chem.* **1997**, *2*, 268–272.
- [57] L. Rulišek, O. Exner, L. Cwiklik, P. Jungwirth, I. Stary, L. Pospíšil, Z. Havlas, *J. Phys. Chem. C* **2007**, *111*, 14948–14955.
- [58] C. Kollmar, R. Hoffmann, *J. Am. Chem. Soc.* **1990**, *112*, 8230–8238.
- [59] Helix, in Wolfram Mathworld. <http://mathworld.wolfram.com/Helix.html>.
- [60] Materials Studio, version 8, Accelrys, San Diego, **2014**.
- [61] H. C. Longuet-Higgins, L. Salem, *Proc. R. Soc. London Ser. A Proc. R. Soc. London Ser. B* **1959**, *251*, 172–185.
- [62] M. Kertesz, C. H. Choi, S. Yang, *Chem. Rev.* **2005**, *105*, 3448–3481.
- [63] R. Zahradnik, in *Nonbenzenoid aromatics* (Ed.: J. P. Snyder), Academic Press Inc., New York, **1971**, pp. 1–80.
- [64] M. Macaluso, C. A. Parish, R. Hoffmann, L. T. Scott, *J. Org. Chem.* **2004**, *69*, 8093–8100.
- [65] Y. Tsuji, R. Hoffmann, *Angew. Chem. Int. Ed.* **2014**, *53*, 4093–4097; *Angew. Chem.* **2014**, *126*, 4177–4181.
- [66] Y. Tsuji, R. Hoffmann, R. Movassagh, S. Datta, *J. Chem. Phys.* **2014**, *141*, 224311.
- [67] a) T. N. Todorov, *J. Phys. Condens. Matter* **2002**, *14*, 3049–3084; b) A. Pecchia, A. D. Carlo, *Rep. Prog. Phys.* **2004**, *67*, 1497–1561; c) G. C. Solomon, C. Herrmann, T. Hansen, V. Mujica, M. A. Ratner, *Nat. Chem.* **2010**, *2*, 223–228.
- [68] N. Tsuji, S. Takajo, H. Aoki, *Phys. Rev. Lett.* **2007**, *75*, 153406.
- [69] S.-H. Ke, W. Yang, H. U. Baranger, *Nano Lett.* **2008**, *8*, 3257–3261.
- [70] Gaussian 09, Revision D.01, M. J. Frisch, G. W. Trucks, H. B. Schlegel, G. E. Scuseria, M. A. Robb, J. R. Cheeseman, G. Scalmani, V. Barone, B. Men- nucci, G. A. Petersson, H. Nakatsuji, M. Caricato, X. Li, H. P. Hratchian, A. F. Izmaylov, J. Bloino, G. Zheng, J. L. Sonnenberg, M. Hada, M. Ehara, K. Toyota, R. Fukuda, J. Hasegawa, M. Ishida, T. Nakajima, Y. Honda, O. Kitao, H. Nakai, T. Vreven, J. A. Montgomery, Jr., J. E. Peralta, F. Ogliaro, M. Bearpark, J. J. Heyd, E. Brothers, K. N. Kudin, V. N. Staroverov, R. Kobayashi, J. Normand, K. Raghavachari, A. Rendell, J. C. Burant, S. S. Iyengar, J. Tomasi, M. Cossi, N. Rega, J. M. Millam, M. Klene, J. E. Knox, J. B. Cross, V. Bakken, C. Adamo, J. Jaramillo, R. Gomperts, R. E. Stratmann, O. Yazyev, A. J. Austin, R. Cammi, C. Pomelli, J. W. Ochterski, R. L. Martin, K. Morokuma, V. G. Zakrzewski, G. A. Voth, P. Salvador, J. J. Dannenberg, S. Dapprich, A. D. Daniels, Ö. Farkas, J. B. Foresman, J. V. Ortiz, J. Cio- slowski, and D. J. Fox, Gaussian, Inc., Wallingford CT, **2009**.
- [71] a) A. D. Becke, *Phys. Rev. A* **1988**, *38*, 3098–3100; b) C. Lee, W. Yang, R. G. Parr, *Phys. Rev. B* **1988**, *37*, 785–789; c) A. D. Becke, *J. Chem. Phys.* **1993**, *98*, 5648–5652; d) P. J. Stephens, F. J. Devlin, C. F. Chabalowski, M. J. Frisch, *J. Phys. Chem.* **1994**, *98*, 11623–11627.
- [72] a) S. Grimme, J. Antony, S. Ehrlich, H. Krieg, *J. Chem. Phys.* **2010**, *132*, 154104; b) E. R. Johnson, A. D. Becke, *J. Chem. Phys.* **2006**, *124*, 174104.
- [73] Y. Zhao, D. G. Truhlar, *Theor. Chem. Acc.* **2008**, *120*, 215–241.
- [74] J.-D. Chai, M. Head-Gordon, *Phys. Chem. Chem. Phys.* **2008**, *10*, 6615–6620.
- [75] J. A. Pople, M. Head-Gordon, *J. Chem. Phys.* **1987**, *87*, 5968–5975.
- [76] H. Schlicke, C. Herrmann, *ChemPhysChem* **2014**, *15*, 4011–4018.
- [77] C. Herrmann, G. C. Solomon, J. E. Subotnik, V. Mujica, M. A. Ratner, *J. Chem. Phys.* **2010**, *132*, 024103.
- [78] Herrmann, L. Gross, T. Steenbock, G. C. Solomon, “Artaios—a code for postprocessing quantum chemical electronic structure calculations”, 2010–2014.

Received: January 5, 2016

Published online on February 17, 2016